General Disclaimer

One or more of the Following Statements may affect this Document

- This document has been reproduced from the best copy furnished by the organizational source. It is being released in the interest of making available as much information as possible.

- This document may contain data, which exceeds the sheet parameters. It was furnished in this condition by the organizational source and is the best copy available.

- This document may contain tone-on-tone or color graphs, charts and/or pictures, which have been reproduced in black and white.

- This document is paginated as submitted by the original source.

- Portions of this document are not fully legible due to the historical nature of some of the material. However, it is the best reproduction available from the original submission.

Planetary Isophotes as a Clue to Aerosol Characteristics

By

George W. Kattawar and Andrew T. Young

Department of Physics
Texas A&M University
College Station, Texas 77843

Report No. 20

December 4, 1975

A paper based on the material in this report has been submitted to Icarus.

Planetary Isophotes as a Clue to Aerosol Characteristics

By George W. Kattawar and Andrew T. Young

ABSTRACT

A study was made to see how much information could be extracted from the Mariner 9 Mars isophotes taken at a phase angle of ~60°. We found that the Minnaert functions and both isotropic and Rayleigh scattering could easily be ruled out, and that it was essential to use forward-peaked phase functions, which were computed from Mie theory. We could achieve isophotes similar to those observed assuming a semi-infinite dust cloud with a considerable variation in particle properties and size distribution, so long as the ratio of the multiply- to singly-scattered light was held within certain limits. These conditions are met by micron-sized, moderately absorbing mineral grains whose mean size should not be _much_ larger than a micron. It was also found that a dust cloud of finite optical thickness bounded from below by a Lambert ground would fit the isophote data.

Planetry Isophotes as a Clue to Aerosol Characteristics

I. Introduction

Spacecraft television systems can, in principle, provide photometric infor-
mation at much better spatial resolution than ground-based telescopes, which are
severely hindered by atmospheric blur (typically, 0.1 planetary radius or worse.)
However, past television systems have failed to produce reliable photometry:
reduced data were found not to be proportional to scene brightness (see, e.g.,
Young, 1974a.) In spite of this quantitative failure, some qualitative infor-
mation remains. In particular, reduced data numbers do seem to have a smooth
monotonic relation to scene brightness, so that the shapes of isophotal contours
in the TV data are approximately correct, even though the numerical values of
each contour level are quite uncertain.

Such contours have been published from Mariner 9 data (Young, 1974a, Fig. 9)
and Venus from Mariner 10 data (Devaux et al, 1975, Fig. 2). In this paper, we
shall concentrate on interpreting the Mars isophotes.

II. The Data

Fig. 1 shows the adopted contours in a standard format. We assume the
north-south symmetry required by the reciprocity principle, and show contours
for only one hemisphere. In this and subsequent figures, the points C,L,M,P,S,
and T are the disk center, the limb, the mirror point the photometric pole,
the subsolar point, and the terminator, respective. The phase angle for
the Mars data is approximately 60°.

We may summarize the principal features of these isophotes as follows:
1.   They are all convex curves; their limb sides are nearly parallel to the limb,
and their terminator sides all curve the same way as the terminator.

2. Each isophote has a rather sharp corner at the junction of its limb and terminator portions. 3. The terminator side of each isophote is much straighter than the limb side, so that they are shaped like a letter D. This is particularly true of the isophotes between the points C and M.

As pointed out by Young (1974a), the position of the maximum brightness is very near the subsolar point, S, which is characteristic of a Lambert photometric function. However, the close adherence of the isophotes to the limb, up to high latitudes, suggests a large single-scattering contribution in the reflected light. If one were to try to use a Minnaert function to describe the brightness distribution, a value of k substantially below unity would be required to produce this limb-brightening effect. But this would displace the peak brightness strongly toward the limb from the subsolar point (see Fig. 2). A Minnaert function with k < 1 is also unphysical, because it produces an infinite brightness at the limb. Therefore a more realistic, physical model is required.

A realistic scattering model involves many parameters. At the very least we need an anisotropic phase function, characterized by the anisotropy and the single-scattering albedo; if a Mie-theory model is used, these are related to the size distribution and the complex index of refraction of the aerosol particles. The size distribution involves at least two parameters (mode size and standard deviation), and so does the refractive index (real and imaginary parts.) It is not clear that so many parameters can be extracted from our data, so we must use any other information available.

It would be very helpful if we knew the absolute level of each isophote, as well as the Bond albedo of the planet at the time of the dust storm. Unfortunately, as Young (1974a) points out, not even the relative intensities of these isophotes are accurately known. Nor is there any accurate estimate of the planet's Bond albedo at the time of the dust storm. However, we can approximate the latter as follows: Young (1974b) has analyzed UBV ground-based

observations of Mars and has shown that a substantial brightening occurs at $L_s \sim 270°$, during the annual dust storm. The average brightening is about 0.3 mag in U, over 0.2 mag in B, and nearly 0.2 mag in V. As the 1971 dust storm was unusually intense, we can expect at least 0.2 mag brightening, and perhaps considerably more, at the time Fig. 1 was obtained.

The average Bond albedo of Mars is about 0.08 in B, 0.15 in V, and 0.25 at 6264Å (Irvine et al., 1968). If we knew the effective wavelength of Fig. 1, we could estimate an average Bond albedo for the planet at this wavelength. According to Young (1974a) the effective wavelength of the B camera for <u>sunlight</u> is about 5590Å. Mars is much redder than the Sun, so the effective wavelength will be greater than this. The average (B-V) color of Mars is about 2/3 of the way from that of a K5 V star to that of a MO III star; according to Ažusienis and Straižys (1966), the effective V wavelengths for these stars are 5540 and 5564Å, respectively, while that for the Sun (G2 V) is 5490Å. According to these figures, the V effective wavelength for Mars would be about 5556Å, or 66Å redder than for the Sun. Since the B camera's effective wavelength for sunlight is 5590Å, we would expect (roughly) a 66Å greater effective wavelength for Mars, or 5656Å. The interpolated Bond albedo at this wavelength is about 0.16.

On the other hand, Leovy et al., (1972) give an effective wavelength for (Mars + the Mariner 9 B Camera) of 5850Å, at which the albedo would be about 0.18. There is considerable uncertainty in the interpolation, because of the nonlinear run of the Martian albedo with wavelength. We adopt 0.17 ± .02 as a reasonable value for the Bond albedo of Mars as seen by the B camera, <u>without</u> a dust storm. The storm probably increased the Bond albedo by at least 0.03, so a minimum value of the Bond albedo, $A_B = 0.20$ is appropriate for our data. Values as large as 0.25 may not be excluded, considering the uncertainties.

II Method of Computation

Referring to Fig. 3, let OE and OS be the direction to the satellite and Sun respectively; SEO the plane defining the intensity equator and also the phase angle α, Q an arbitrary point on the planetary surface where OQZ defines the vertical at point Q. .It is also convenient to introduce the planetary co-ordinates ζ(longitude) and η(colatitude).

The angles of incidence and reflection can be expressed as

$$\cos \theta_0 = \mu_0 = \sin \eta \cos(\zeta-\alpha) \tag{1}$$

$$\cos \theta = \mu = \sin \eta \cos \zeta, \tag{2}$$

where θ_0 and θ are acute angles.

The azimuthal angle ϕ for the reflected ray is given by

$$\cos \phi = (\cos \theta_0 - \cos \alpha)/\sin \theta \sin \theta_0 \tag{3}$$

and

$$\sin \phi = \sin \alpha \cos \eta \sin \theta/\sin \theta_0 . \tag{4}$$

The x and y coordinates of the projection of point Q on the plane OPG are given by

$$x = \sin \eta \sin \zeta \tag{5}$$

and

$$y = \cos \eta, \tag{6}$$

where we have assumed a planetary radius of unity.

To generate isophotes, we used a grid in x and y coordinates, related to μ and μ_0 by

$$\mu = [1 - (x^2 + y^2)]^{1/2}, \tag{7}$$

and

$$\mu_0 = \mu \cos \alpha + x \sin \alpha. \tag{8}$$

Once μ, μ_0, and ϕ have been determined, the reflected intensity I (μ, μ_0, ϕ) can be found for the point (x,y). The intensities were computed by the matrix operator routine described by Plass et al., (1973). To insure adequate resolution in both μ and ϕ, twenty-one Lobatto points were used for the μ coordinate, and nineteen equally-spaced azimuthal angles ($\Delta\phi = 10^0$) were used for the ϕ coordinate in the computation of the reflected intensities.

As an aid in interpreting the data, isolines of μ, μ_0 and ϕ are presented in Fig. 4. They were computed by the following procedure. Rewriting Eq. (7) we get

$$x^2 + y^2 = 1 - \mu^2 . \tag{9}$$

This shows that the isolines of μ are circles, centered at the center of the disk and having a radius of $(1 - \mu^2)^{1/2}$. Now eliminating μ from Eqs. (7) and (8) we get

$$\frac{(x - \mu_0 \sin \alpha)^2}{\cos^2\alpha} + y^2 = (1 - \mu_0^2). \tag{10}$$

This shows that the isolines of μ_0 are ellipses whose centers are located at $(\mu_0 \sin \alpha, 0)$. The ratio of the major to minor axes of these ellipses is $(\cos \alpha)^{-1}$. For the phase angle of 60^0 shown in Fig. 4 this ratio is simply 2:1. It should be noted that the isolines of μ_0 are also isophotes for a Lambert surface since the intensity for a Lambert surface is proportional to μ_0. The isolines of ϕ are more difficult to compute and the following technique was used. We have:

$$\tan 0/2 = \cos [(\phi - \beta)/] \tan [(\alpha - 0_0)/2]/\cos [(\phi + \beta)/2] \tag{11}$$

and

$$\sin \theta_0 = \sin \beta \sin \alpha / \sin \phi. \qquad (12)$$

First the angles ϕ and β were chosen, and Eq. (12) was used to compute θ_0. These values were then used in Eq. (11) to compute the angle θ. Once θ and θ_0 have been computed then the x and y coordinates can easily be calculated from Eqs. (7) and (8). A similar technique was used by SeKera and Viezee (1961).

The phase functions used in this study were generated from Mie theory with a program developed by Kattawar and Plass (1967), using a particle size distribution of the form

$$n(r) \propto r^\alpha \exp(-br^\gamma), \qquad (13)$$

which Deirmendjian (1969) called a modified gamma distribution. The mode radius is

$$r_c = (\frac{\alpha}{\gamma b})^{1/\gamma}. \qquad (14)$$

The spherical or Bond albedo A_B can easily be computed from the reflected flux $F_R(\mu_0)$, for an incident solar flux of unity, by

$$A_B = 2 \int_0^1 F_R(\mu_0) d\mu_0. \qquad (15)$$

Now if one knows the Bond albedo for a certain phase function with single scattering albedo $\tilde{\omega}_1$, then one can use the similarity relations of Van de Hulst (1968) to relate it to another phase function with single scattering albedo $\tilde{\omega}_2$ by

$$\frac{1 - \tilde{\omega}_1}{1 - g_1} = \frac{1 - \tilde{\omega}_2}{1 - g_2} \qquad (16)$$

where g, the so-called asymmetry factor, is related to the phase function $P(\cos \theta)$ by $g = \int_{-1}^1 P(\cos \theta) \cos \theta \, d(\cos \theta) / \int_{-1}^1 P(\cos \theta) \, d(\cos \theta)$. (17)

It should be noted that Eq. (16) is only approximate, and the error becomes worse as $\tilde{\omega}$ decreases. When $\tilde{\omega}$ is close to unity it is quite accurate.

IV. Discussion of Models

The model isophotes are presented in a uniform format. The contour in-
terval is 0.08 of the maximum brightness of each model; the relative brightness
levels are thus 0.08, 0.16..., 0.88, and 0.96. The 0.48 contour, which has
half the brightness of the brightest contour, is emphasized. To show more de-
tail near the peak, the 0.92 contour level is usually added as a dashed line.
Thus the 12 solid and 1 dashed contours are comparable to the 14 solid contours
in Fig. 1. Only one hemisphere is shown; the other would be its mirror image.

Fig. 2 compares several very simple models. The top row shows isophotes
for Minnaert functions; the middle shows isotropic-scattering models; and the
bottom row shows Rayleigh-scattering models. As mentioned above, the Minnaert
functions fail to reproduce the data. A further problem is that a Minnaert
function has no definite albedo, so this information cannot be used.

Isotropic-scattering models of infinite optical depth were proposed by
Leovy, et al. (1972). According to them, a single-scattering albedo $\tilde{\omega}_0$ of about
0.7 can reproduce the surface brightness measured by the B camera. However, a
subsequent investigation of the TV photometry (Young, 1974a) casts doubt on the
reliability of the data on which this result was based. Fig. 2f shows that the
shape of the isophotes calculated for a semi-infinite isotropic-scattering model
with $\tilde{\omega}_0 = 0.7$ bears no resemblance whatever to the observed shapes, which are
unaffected by the nonlinearity of the data. However, the Bond albedo for this
model (0.26) is acceptable.[*] The conclusion of Leovy et al. (1972) that isotropic
scattering produces a quasi-Lambertian photometric function for such a low

_____

*The Bond albedo of the $\tilde{\omega}_0 = 0.7$ model is about 50% brighter than the albedo with-
out a dust storm. Thus, the albedo derived for the dust by Leovy et al. (1972) is
inconsistent with their statement that "the dusty Mars is not significantly
brighter than the clear Mars."

single-scattering albedo is clearly wrong. Fig. 2d shows that quasi-Lambertian behavior does occur for <u>conservative</u> isotropic scattering: however, even Fig. 2e, with a Bond albedo roughly twice that of Mars, is far from Lambertian.

These isotropic models already show the advantages of using isophotes, rather than the unreliable Mariner photometry, as a basis for studying the optical properties of the dust. Clearly, no isotropic-scattering model will fit the data.

Another simple (but more plausible) model is Rayleigh scattering. Although the optical depth of the molecular atmosphere of Mars is only about 3×10^{-3}, very small dust particles could produce nonconservative Rayleigh scattering. However, as the single-scattering phase function is not very different from isotropic, we do not expect the computed isophotes to be much like those observed. Figs. 2 g-i confirm this expectation. Conservative Rayleigh scattering, like conservative isotropic scattering, produces quasi-Lambertian isophotes; but models with plausible Bond albedos are much too bright at the limb.

Both of the conservative-scattering models (Figs. 2d and 2g) have their maximum brightness closer to the mirror-point M than for a Lambert surface, whose maximum is at S, the sub-solar point. In these models, most of the observed light (which is quasi-Lambertian in distribution) is multiply-scattered. The ratio of multiple- to single-scattered intensity for the brightest point (MS/SS) is 6.7 for $\tilde{\omega}_0 = 1.0$, whereas for $\tilde{\omega}_0 = 0.80$ and 0.5710 it is 1.8 and 1.4 respectively. Hence, increasing the importance of single scattering should move the maximum to S <u>and</u> produce limb brightening. Not only do the observed isophotes indicate a moderate brightening toward the limb, but the non-conservative isotropic and Rayleigh models of low Bond albedo show strong limb brightening, due to a much smaller multiple- to single-scattering ratio. We need a low-albedo model that has relatively less single-scattering backward at 60° phase angle. Any forward-scattering phase function should do this.

In order to use Mie-scattering models we have to choose both the complex refractive index and the size distribution. In Figs. 5a - 5c the size distribution is fixed and the refractive index is varied. The phase functions for these models are shown in Fig. 6a. In Fig. 5a the Bond albedo is too high and the isophotes are too rounded, due to the large value of MS/SS = 36.2. To decrease the Bond albedo, we increased N_2 (Fig. 5b) and thus decreased $\tilde{\omega}_0$ and reduced the MS/SS ratio to 16.3. This reduction is due entirely to the diminution of the multiple-scattering, since the single scattering contribution is approximately the same for the two models (see Fig. 6a). Consequently, the brightest isophote moves closer to the limb and has a more realistic D shape, while the Bond albedo decreases to the estimated value during the dust storm. In Fig. 5c we increased the real part of the refractive index, and adjusted the imaginary part to keep the Bond albedo in agreement with Fig. 5b. The isophotes are shifted more toward the limb and extend higher in the vertical direction; also, the MS/SS ratio has been reduced to 8.5, which is largely due to the increase in the single scattering contribution (see Fig. 6a). In Figs. 5e and 5f we set the real part of the refractive index to 1.5 and varied the size distribution. The mode radii for the two cases are 0.5 μm and 0.2 μm respectively (see Fig. 6a for the phase function). For both of these models the isophotes are too rounded at the top. The smaller sizes also shift the bright point towards the terminator.

It should also be noted that using the similarity relations of Van de Hulst (1968) can lead to erroneous results. For example, in Figs. 5e and 5f the ratio $(1 - \tilde{\omega}_0)/(1 - g)$ for the two cases is 0.25 and 0.24 respectively. This relation is useful for matching Bond albedo data, but is useless for isophote matching; this conclusion was already reached by Kattawar (1975). An extreme example can be seen by comparing Figs. 5e, 5f and 2h. For the Rayleigh case $(1 - \tilde{\omega}_0)/(1 - g) = 0.2$ and gives the same Bond albedo, but the isophotes bear no resemblance to those in Figs. 5e and 5f.

We next used a size distribution of $r^6 e^{-12r}$, which has a mode radius of 0.5 μm, and increased the real part of the refractive index to 2.0. This has the effect of increasing the single scattering at 120° scattering angle (compare Figs. 6a and 6b). This gives the same Bond albedo as that of Fig. 5e with the same distribution but $N_1 = 1.5$. The effect of this (see Fig. 7c) is to shift the maximum toward the limb and produce less rounding of the isophotes at higher latitudes. To bring the Bond albedo down to a more realistic level we increased N_2 (see Fig. 7d). The MS/SS ratio is reduced and the isophotes are shifted even more toward the limb and are actually starting to become concave.

In all of the models we have considered to this point, we have assumed the optical thickness to be infinite. Although the observed isophotes in the subsolar area are quite uncertain, both because of the low brightness gradients and the large residual-image effects, we suspect that effects of finite optical thickness may appear there, as the total air mass is least at the mirror point. We therefore explored the effect of a finite optical thickness on the shape of the isophotes. We used the model in Fig. 7d and first set $\tau = 4$ with a perfectly absorbing ground (i.e., the ground albedo $A_G = 0.0$.) The results are shown in Fig. 8a. The Bond albedo is in an acceptable range, but the isophotes are pushed much too close to the limb, and have become concave over a region from the mirror-point to the sub-solar point. We next set $A_G = 0.5$, assuming a Lambert ground, and the Bond albedo increased only by 6%. However, the change in the isophotes was remarkable (see Fig. 8b). In fact, this case gave reasonably good agreement with the actual isophotes. We considered two additional cases, namely $A_G = 1.0$ and a perfectly antispecular ground (see Figs. 8c and 8d). In each of these cases the isophotes are too rounded.

Conclusion

The isophotes mainly tell us the ratio of multiple to single scattered light at our phase angie. We can achieve isophotes similar to those observed with a considerable variation in particle properties and size distribution, so long as this ratio is achieved, and the Bond albedo is not unreasonable. These properties are satisfied by micron-sized, moderately-absorbing mineral grains. We believe that the mean particle size should not be much larger than a micron, for this would make too much forward scattering and put the maximum brightness on the limb side of the sub-solar point.

Acknowledgment

References

Ažusienis, A., and Straižys, V. (1966). The correction of response curves and parameters of the U, B, V systems. I. Response curves. *Bull. Vilnius Astron. Obs.*, No. 16, 3.

Deirmendjian, D. (1969), Electromagnetic Scattering on Spherical Polydispersions, American Elsevier Publishing Company, Inc. New York.

Devaux, C., Herman, M., and Lenoble, J. (1975). Interpretation of the photometric measurements of Venus by Mariner 10. *J. Atmos. Sci.* 32, 1177-1189.

Irvine, W., Simon, T., Menzel, D., Pikoos, C., and Young, A. (1968). *Astron. J.* 73, 807-828.

Kattawar, G. W., and Plass, G. N. (1967). Electromagnetic scattering from absorbing spheres, *Appl. Opt.* 6, 1377-1382.

Kattawar, G. W. (1975). A Three-Parameter Analytic Phase Function for Multiple Scattering Calculations, *J. Quant. Spec. Rad. Trans.* 15, 839-849.

Leovy, C., Briggs, G., Young, A., Smith, B., Pollack, J., Shipley, E., and Wildey, R. (1972). The Martian Atmosphere: Mariner 9 Television Experiment Progress Report, *Icarus* 17, 373-392.

Plass, G. N., Kattawar, G. W., and Catchings, F. E., (1973). Matrix Operator Theory of Radiative Transfer: Rayleigh Scattering, *Applied Optics* 12, 314-329.

Sekera, Z., and Viezee, W., (1961). Distribution of the Intensity and Polarization of the Diffusely Reflected Light Over a Planetary Disk. Rand Report R-389-PR.

Van de Hulst, H. C. (1968). Asymptotic fitting, a method for solving anisotropic transfer problems in thick layers. *J. Comp. Phys.* 3, 291-306.

Young, A.T., (1974a). Television Photometry: The Mariner 9 Experience. *Icarus* 21, 262-282.

Young, A. T., (1974b). UBV Photometry of Mars. In IAU Symposium 65, "Explora-

tion of the Planetary System," (A. Woszczyk and C. Iwaniszewska, eds.)

D. Reidel Publishing Co., Dordrecht, pp. 253-286.

Figure Captions

Figure 1. Mariner 9 isophotes of Mars during dust storm, at a phase angle 60°.

Figure 2. a-c: Computed Isophotes for Minnaert functions, where the intensity is assumed proportional to $\mu_0^k \mu^{k-1}$ for k $=$ 0.9, 0.8, and 0.7, respectively. d-f: Isophotes for a semi-infinite isotropic scattering atmosphere with single scattering albedos $\tilde{\omega}_0$ = 1.0, 0.9, and 0.7 respectively: g-i: Isophotes for a semi-infinite Rayleigh scattering atmosphere with $\tilde{\omega}_0$ = 1.0, 0.8, and 0.57 respectively.

Figure 3. Planetary coordinates used for computation.

Figure 4. Isolines of μ, μ_0, and ϕ for a phase angle of 60°. The isolines of μ_0 are isophotes for a Lambert surface.

Figure 5. Isophotes for various Mie scattering models assuming a semi-infinite cloud. a-c: $n(r) \propto r^6 e^{-6r}$ and N_1 = 1.5, N_2 = 0.001; N_1 = 1.5, N_2 = 0.004; and N_1 = 1.65, N_2 = 0.005 respectively. d: Mars data. e: $n(r) \propto r^6 e^{-12r}$, N_1 = 1.5, N_2 = 0.005. f: $n(r) \propto r^6 e^{-30r}$, N_1 = 1.5, N_2 = 0.013.

Figure 6. a-b: Phase functions computed from Mie theory for use in isophote computations.

Figure 7. a-b: Same as Figs. 5e and 5d respectively. c-d: $n(r) \propto r^6 e^{-12r}$ and N_1 = 2.0; N_2 = 0.0055, N_2 = 0.01 respectively.

Figure 8. Isophotes showing the effects of a finite optical depth, τ = 4, over both a Lambert surface (a-c) and an antispecular surface, (d).
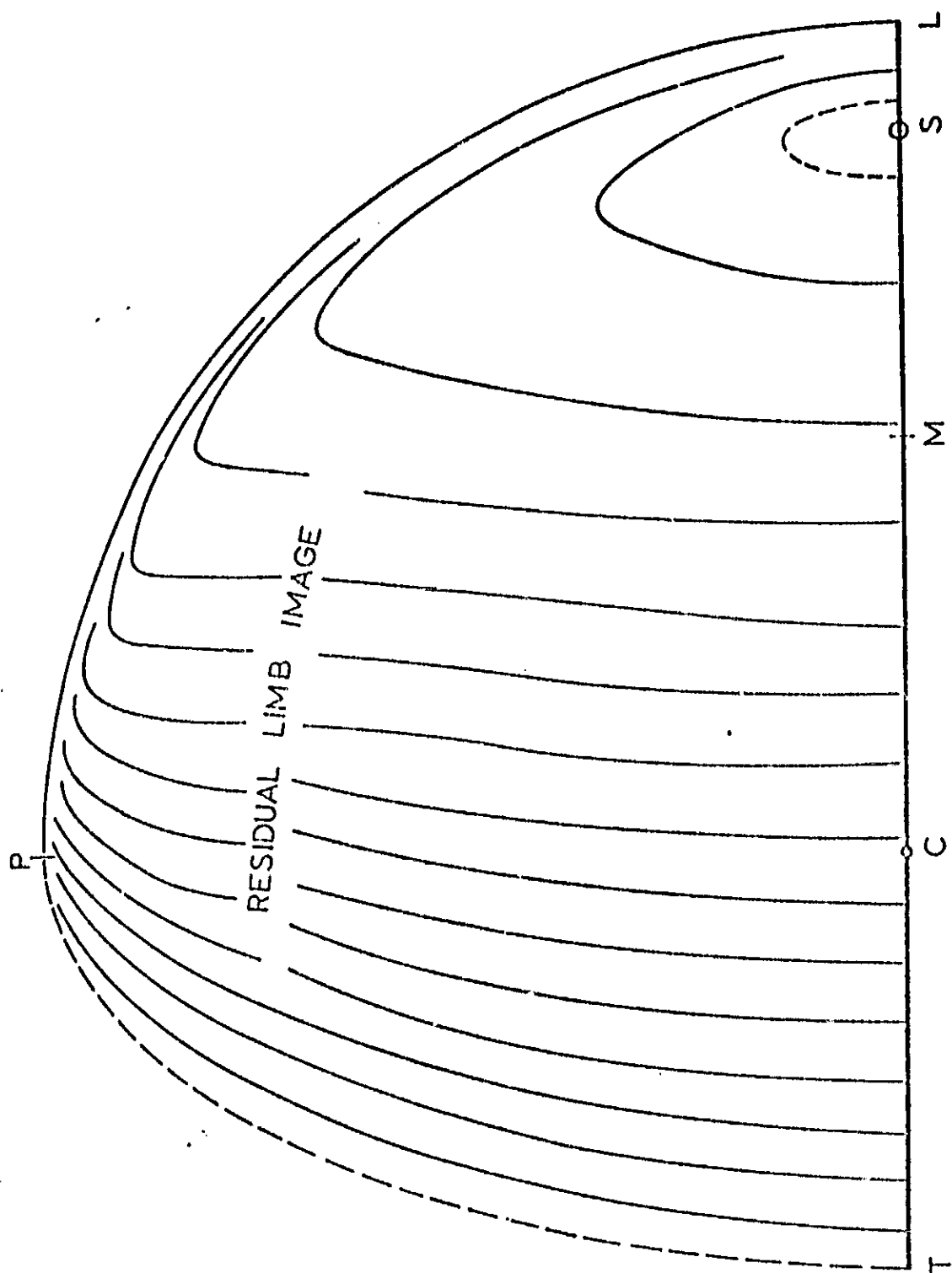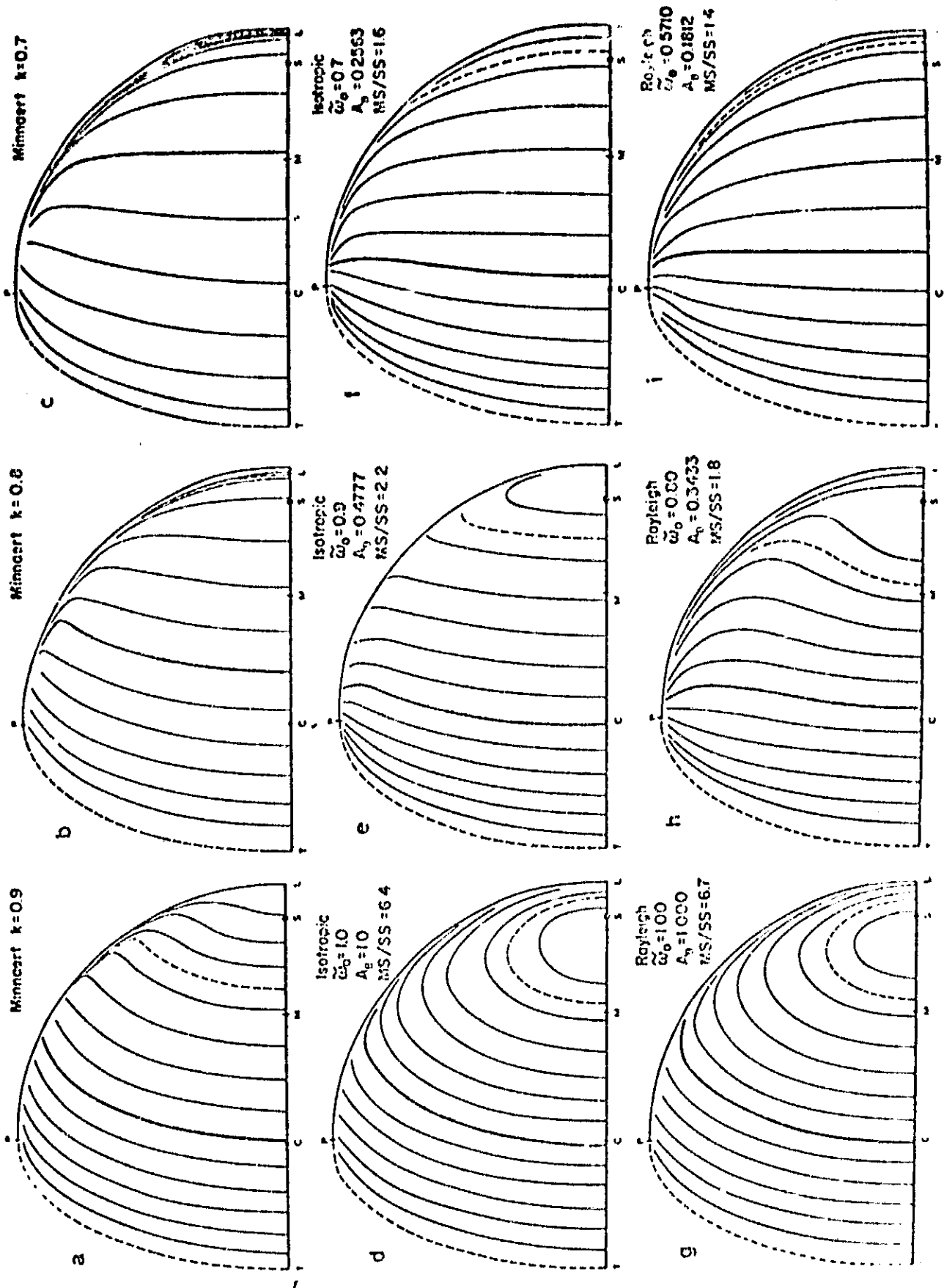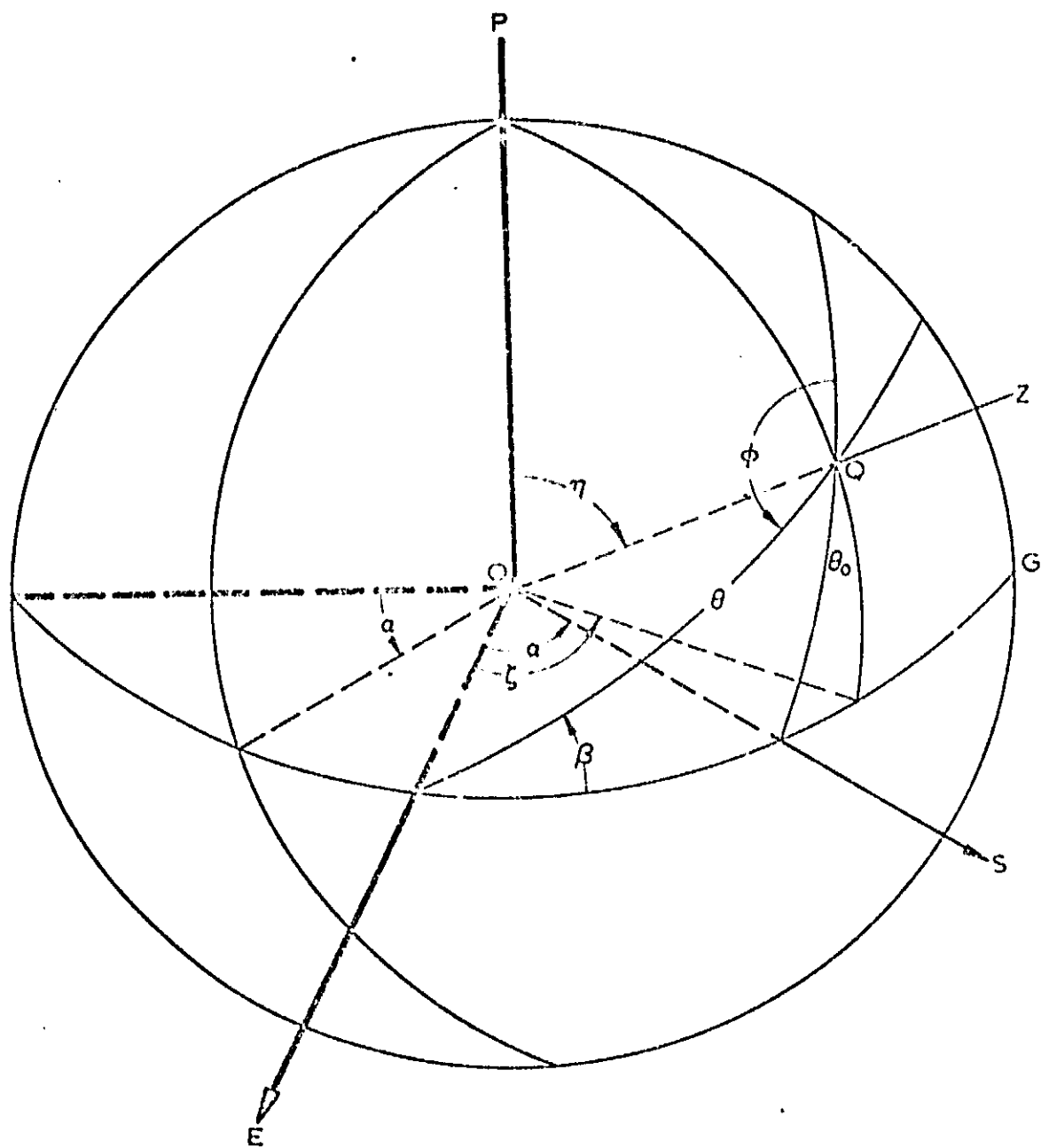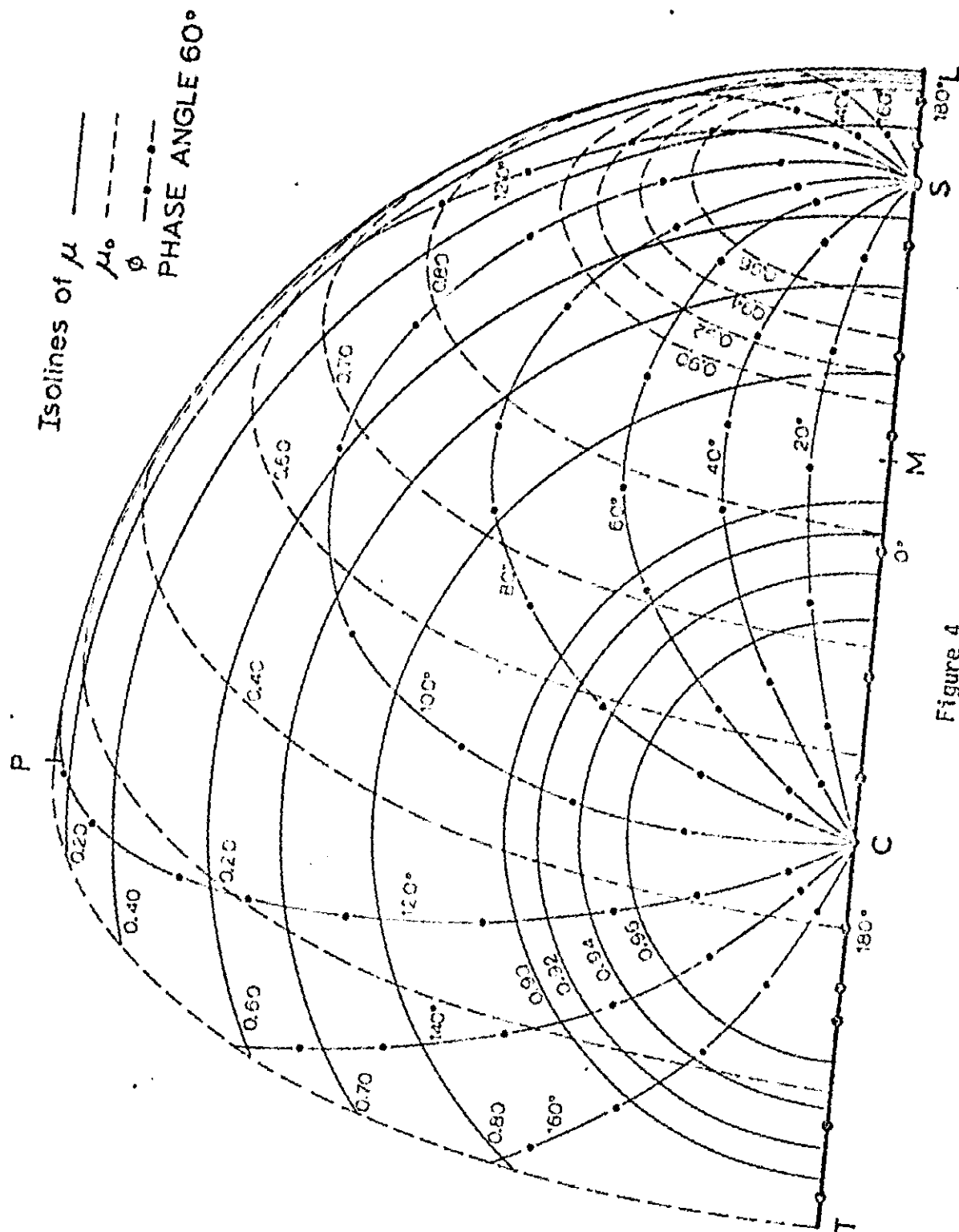
RESIDUAL LIMB IMAGE

Figure 1

Figure 2

Minnaert k=0.9 | Minnaert k=0.8 | Minnaert k=0.7

a | b | c

Isotropic
$\tilde{\omega}_0 = 1.0$
$A_0 = 1.0$
MS/SS = 6.4

Isotropic
$\tilde{\omega}_0 = 0.9$
$A_0 = 0.4777$
MS/SS = 2.2

Isotropic
$\tilde{\omega}_0 = 0.7$
$A_0 = 0.2563$
MS/SS = 1.6

d | e | f

Rayleigh
$\tilde{\omega}_0 = 1.000$
$A_0 = 1.000$
MS/SS = 6.7

Rayleigh
$\tilde{\omega}_0 = 0.90$
$A_0 = 0.3433$
MS/SS = 1.8

Rayleigh
$\tilde{\omega}_0 = 0.5710$
$A_0 = 0.1812$
MS/SS = 1.4

g | h | i

Figure 3

Figure 4

Isolines of μ
μ_0
ϕ
PHASE ANGLE 60°

Figure 5

Figure 6

Figure 7

b

$n(r) \propto r^8 e^{-12r}$
$N_1 = 2.0, \ N_2 = 0.01$
$\bar{\omega}_0 = 0.842$
$A_3 = 0.2401$

$\tau = 4$
$A_6 = 0.5$

d

Antispacier $\tau = 4$ $n(r) \propto r^8 e^{-12r}$ $N_1 = 1.0, \ N_1 = 2.0, \ N_2 = 0.01$
$A_6 = 1.0$
$\bar{\omega}_0 = 0.642$
$A_3 = 0.2555$

a

$n(r) \propto r^8 e^{-12r}$
$N_1 = 2.0, \ N_2 = 0.01$
$\bar{\omega}_0 = 0.6420$
$A_3 = 0.2258$
$k S / S S = 4.8$

$\tau = 4$
$A_6 = 0.0$

c

$n(r) \propto r^8 e^{-12r}$
$N_1 = 2.0, \ N_2 = 0.01$
$\bar{\omega}_0 = 0.642$
$A_3 = 0.2555$

$\tau = 4$
$A_6 = 1.0$

Figure 8